Clockwork Orangutan: microRNAs, thermoregulatory tradeoffs, and the evolution of brain size

Bastian Fromm, PhD**
UiT - The Arctic University of Norway,
The Arctic University Museum of Norway
9006 Tromsø, NO

Thomas Sorger, PhD*
Department of Biology
Roger Williams University
Bristol, RI 02809

* Lead contact
** Second corresponding author

ABSTRACT

Models of brain size evolution have yet to account for the thermoregulatory adaptations that enabled a four-fold increase in brain metabolic rate (*MR*) in the hominid lineage. We postulated a mammalian Core (kidney + heart + liver + brain), analogous to the thermogenic core in a biophysical model of endothermy (Porter and Kearney, 2009), and demonstrate that the sizes of the brain, the primary consumer of glucose, and the liver, the primary organ of gluconeogenesis, have varied inversely relative to this Core. We inferred organ cellular metabolic rates (*cMR*s) based on the parallel adaptive increases in *MR*/kg and number of microRNA families (*mirFam*) that have characterized major shifts in mammalian evolution: the advent of placentation, the emergence of permanent homeothermy, and the divergence of Catarrhini. Again, the *cMR* of the liver varied inversely with the *cMR*s of kidney, heart and brain, a phylogenetic plasticity that appears to recapitulate the liver's unique developmental plasticity. With *mirFam* as a proxy for energy reliability, a positive feedback model of relative brain size detected adaptation to a low-energy regime among the smallest primates and, among the largest primates, adaptation to the physiological limit on the rate of heat dissipation. A key observation is that the energy consumption of the brain per unit mass declines strictly as an exponential function of body size, regardless of phylogeny. The *cMR* approach extends the critical analysis of log-based allometry in a new direction, uncovering a rich network of relationships among *mirFam*, body size, metabolic rate, temperature, and thermal conductance.

INTRODUCTION

With the emergence of permanent homeothermy Boreoeutheria crossed a threshold of energy reliability relative to earlier-branching placentals and marsupials, among which many orders exhibit some degree of heterothermy[1-2], and set the stage for the subsequent ecological diversification of Laurasiatheria and Euarchontoglires[3]. The divergence of Boreoeutheria corresponded to adaptive increases in specific *MR* (resting $MR/M^{0.75}$) and body temperature (T_b), independent of body size, that coincided with a significant increase in the number of microRNA families (*mirFam*)[4]. Conversely, subsequent reappearances of heterothermic species have been accompanied by reductions in *mirFam*[4-6]. The evolutionary expansion of brain size in the human lineage also depended on significant increases in *rMR*[8-9] and was accompanied by a 15% increase in *mirFam*[6]. Thus, each increase in the range of *mirFam* has defined a new range of variation of *rMR* and *Mbdy* and, consequently, the potential range of brain size variation.

Cassidy et al (2019)[7] first demonstrated a relationship between *rMR* and *mirFam* during *Drosophila* development. While differentiation of the eye depended on microRNA activity in wild type *Drosophila*, development proceeded normally without microRNAs when flies were engineered to have slower *MR*s, doubling the time to eclosion. The authors reasoned that the normal unfolding of eye development must

depend on the transient expression of transcription factors and the timely decay of their concentrations. In order to maintain these evolutionarily conserved rates of decay, flies with wild type *MR*s and rates of protein synthesis depend on microRNA-mediated repression[7]. By extension, the adaptive increases in *mirFam* that have accompanied mammalian shifts to faster *rMR*s may have served to maintain synchrony among gene regulatory networks (GRNs).

Simulation of two million years of African and Eurasian climate and habitats supports the view that *H. sapiens* evolved from *H. heidelbergensis* in southern Africa during an unusually warm period that would have required adaptation to the hotter, drier conditions[10] envisioned by the "Savanna hypothesis"[11-13]. Among hunter-gatherers and contemporary indigenous populations, both resting and active *MR*s are elevated in comparison with those of non-human apes, necessitating faster rates of heat dissipation[9]. Such cooling has been enabled by uniquely human adaptations such as hairlessness, bipedalism, and a 10-fold increase in the density of eccrine sweat glands relative to the densities found in chimpanzees and macaques[14]. Nevertheless, human brain temperature increases during exercise in parallel with that of the body core, eventually leading to hyperthermia and fatigue[15]. Unlike arid-zone artiodactyls such as springbok, primates lack a carotid *rete*, a counter-current structure that can decrease brain temperature up to 0.5°C in animals at rest[16-17]. On the other hand, heat dissipation may be one potential benefit of the so-called "oxygen paradox" of neurovascular coupling *i.e.* the surplus blood flow in excess of oxygen demand, elicited by neuronal activation[18-20].

Another potential mechanism to address the thermoregulatory challenge of a larger brain, first proposed four decades ago, is a tradeoff in energy expenditure between the brain and another metabolically expensive tissue, such as kidney, heart, liver or intestine[21-22]. However, attempts to detect the tradeoff predicted by this "expensive tissue hypothesis" were abandoned following publication of an influential report encompassing 100 species, including 23 primates, that found no significant anticorrelations among the body mass-independent residuals of seven metabolically expensive organs[23]. In a seminal study, Lande (1979)[24] attributed the evolutionary increase in primate brain size to a genetic uncoupling of its dependence on body size. We postulated that thermal homeostasis could be achieved by relaxing this constraint on the sizes of all four major thermogenic organs (kidney, heart, liver, and brain) with respect to a composite 4-organ "Core", analogous to the thermogenic core in the biophysical model of Porter and Kearney (2009)[25]. Relative to this Core, we find that increases in the proportion of the brain have been offset by decreases in the proportion of the liver over the evolutionary history of mammals. We demonstrate that, unlike the conventional index of brain size, log *Mbrain*/log *Mbody*, organ/Core mass ratios fulfill two conditions required in order to detect

energy-based tradeoffs: they reflect the relative energy cost *in the individual animal,* and they exhibit normal distributions, the outcome of selection for thermal homeostasis.

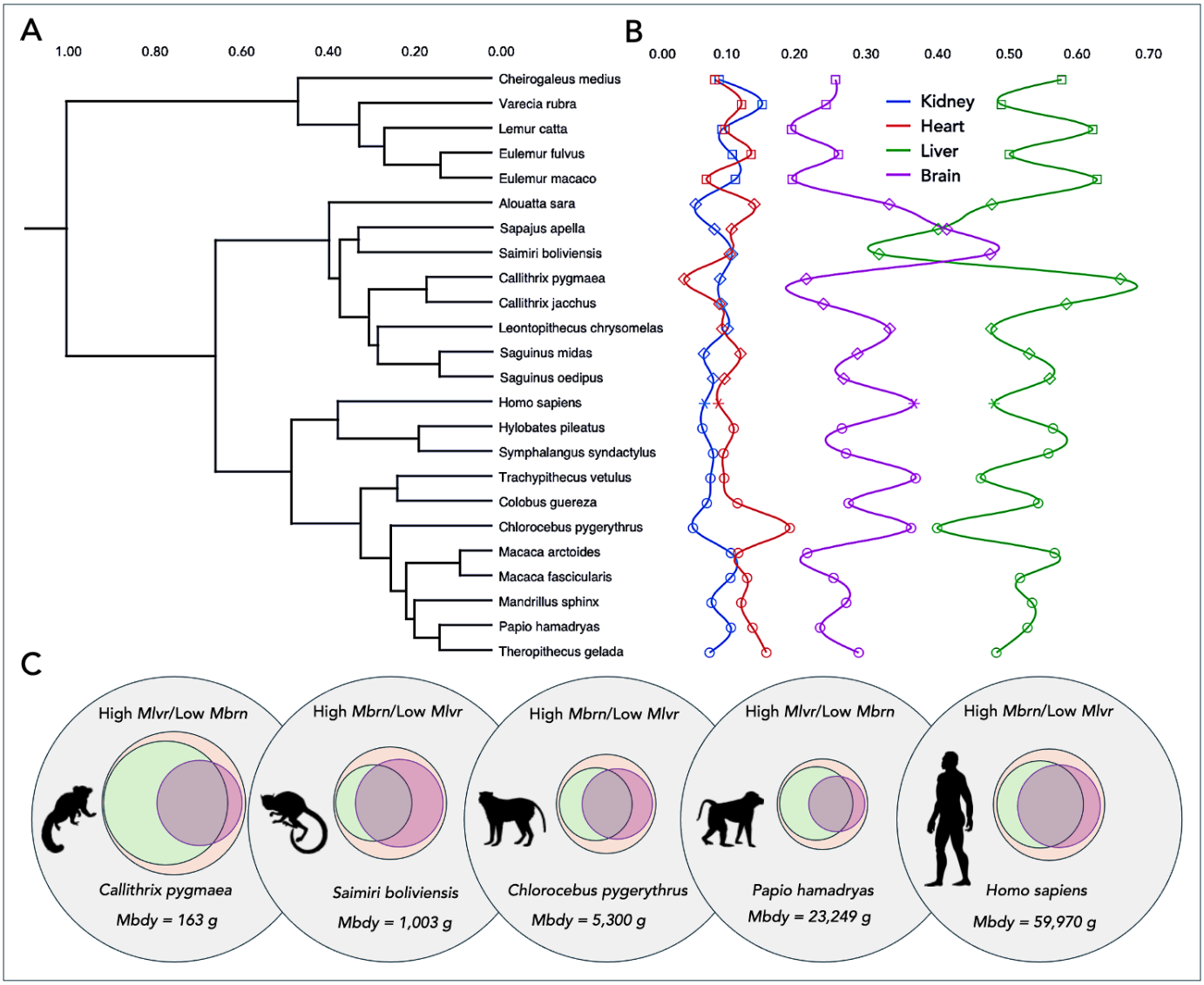

Figure 1. The proportion of brain mass in the thermogenic Core varies reciprocally with that of the liver.
A. Ultrametric time tree of 24 primates[26]. The scale bar represents the relative time of divergence.
B. Mass proportion of each organ relative to the total Core mass.
C. Summary comparing representative species with relatively low or high ratios of brain/liver mass. The radius of each inner circle represents a spherical volume proportional to organ or Core mass. The relative sizes of liver and brain are represented by green and purple circles, respectively. Silhouettes: *Callithrix jacchus*, *Saimiri* (generic), *Erythrocebus patas*, *Papio* (generic), *Homo sapiens idaltu* (© Phylopic 2024, compiled by T. Michael Keesey.

In order to compare the rates of heat production of the four organs in our proposed thermogenic Core, we inferred their cellular *MR*s (*cMR*s) based on three criteria:

a) correlation with *mirFam* and organ size (physiological relevance)[4];

b) equivalence between the joint *cMR* of the four Core organs and the predicted rate of

core thermogenesis, which scales as ~ $\sqrt{M}$ (thermodynamic relevance)[25];

c) utility for the unsupervised classification of major primate clades (phylogenetic relevance).

We find that liver *cMR*s are strictly anticorrelated with body mass and the *cMR*s of kidney, heart and brain. Since the liver is the primary organ of gluconeogenesis during fasting or starvation, the tradeoff between liver and brain led us to formulate a positive feedback model of brain size evolution governed by energy reliability, following previous suggestions[27-28].

RESULTS

The proportion of brain mass in the Core varies reciprocally with that of liver

Of the six possible tradeoffs among four thermogenic organs, two have occurred consistently among primates, that between brain and liver, and a dampened tradeoff between heart and kidney (Figure 1-B). Similar tradeoffs were observed among Glires, Laurasiatheria, Marsupialia, and an Afrotherian (Supplementary Figures S1 and S2). Relative to the *Mbrn*/*Mcor* ratio in the human (0.36), higher mass ratios (> 0.40) were observed in the smallest weasel (*Mustela nivalis*, 0.43), a squirrel (*Sciurus vulgaris*) (0.41), and the 1-kg squirrel monkey, *Saimiri boliviensis* (0.47) (Figure 1-C). In contrast, when standardized to body mass, the *Morg*/*Mbdy* ratios of all four thermogenic organs covaried strongly, regardless of phylogeny (Supplementary Figure S3).

A tradeoff between liver and brain mass was also readily demonstrable in log-transformed data, provided that they were ranked according to Core mass, rather than body mass (Figure 2-C *versus* Figure 2-A). The tradeoff was most apparent when the periodic pattern of variation of the mass-independent residuals of each organ wss plotted in the species rank order of Core mass (Figure 2-D), rather than body mass (Figure 2-B), accounting for the inability of the previous major test, using the same dataset, to detect these tradeoffs[23].

Physiologically-based cMRs do not correspond to log-based sMRs

Assuming power law models, we distinguish between conventional log-based specific *MR*s (*sMR*s):

$\boldsymbol{sMR = j \times M^b}$, where *b* is the slope of log *rMR*/log *M*,

and celluar *MR*s (*cMR*s)[4]:

$\boldsymbol{cMR = k \times M^c}$, where *c* is the allometric exponent obtained by maximum likelihood fitting of rMR/M^c to a physiologically-relevant trait with a normal distribution, such as *mirFam*.

An *sMR* model is the indirect outcome of correlational selection on mass and *rMR*[29], and the relationship between log *rMR* and log mass is a function of many interacting factors, anatomic and physiological, that are

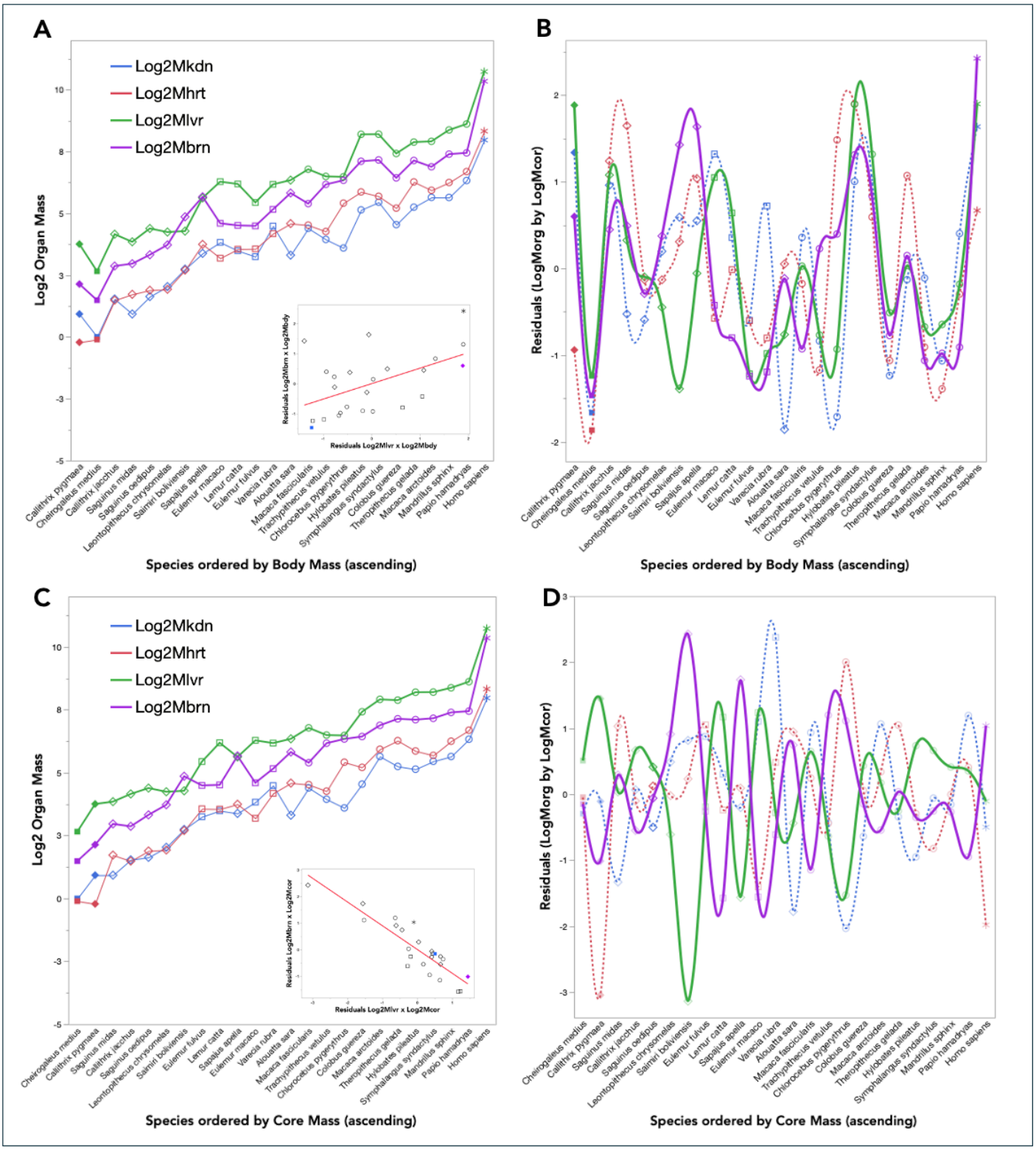

Figure 2. Variation of liver and brain mass relative to either body mass or the mass of the four-organ Core. A and C: Variation of organ size relative to body mass and Core mass in primates (N = 24). Inset graphs: conventional plots of log *Mbrn* residuals *versus* log *Mlvr* residuals from regressions on either Log *Mbdy* (A: R^2 = 0.23, P = 9.63e-03), or Log *Mcor* (C: R^2 = 0.79, P = 5.03e-09). Filled symbols = heterotherms. B and D: Mass-independent residual variation relative to body mass (B) and Core mass (D) among primates.

only indirectly related to thermal homeostasis. *mirFam*-based *cMR*s are sensitive to body temperature and robust to variation in the range of mass[4], consistent with a direct relationship to rates of thermogenesis, a mass-independent intensive property.

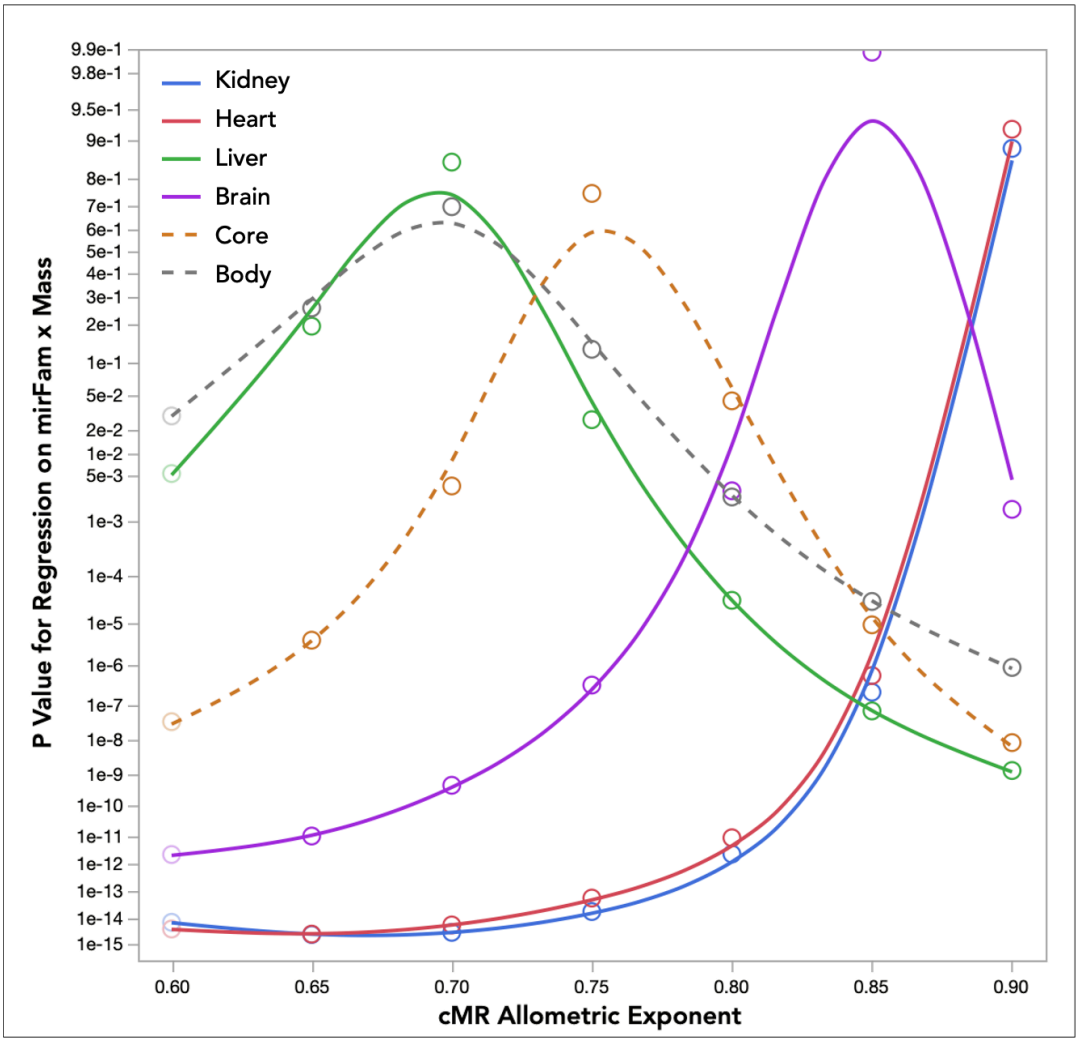

Figure 3. Dependence of organ *cMR*s on *mirFam* and √*Morg* ($Morg^{0.5}$) (51 Euarchontoglires). *P* values for regressions of organ *cMR* on √*Morg* and *mirFam*. Curves were fit by the cubic spline method. Note that the range $M^{0.70}$ - $M^{0.80}$ defines a zone of minimal correlation for the Core *cMR,* centered at $M^{0.75}$. *cMR*s were regressed on √*Morg* rather than log *Morg*, yielding *P* values several orders of magnitude lower. Regression on *mirFam* alone, without correction for organ mass, yielded the similar patterns, the only difference being a shift in the peak of the distribution of *P* values for *cMRbdy* from $M^{0.70}$ to $M^{0.75}$.

Inference of thermogenic organ cMRs

The context for our approach is that the variation of mammalian *cMR*s with respect to *mirFam* best fits a model of stabilizing selection when *rMR*s are scaled to the evolutionarily conserved Kleiber exponent of 0.75, *i.e.* $cMR.75bdy = rMRbdy/Mbdy^{0.75}$ [4, 30]. In order to estimate the *cMR* of each of the four thermogenic organs, we compared the dependence of rMR/M^{exp} on *mirFam* and organ mass for exponents in the range 0.60 - 0.90

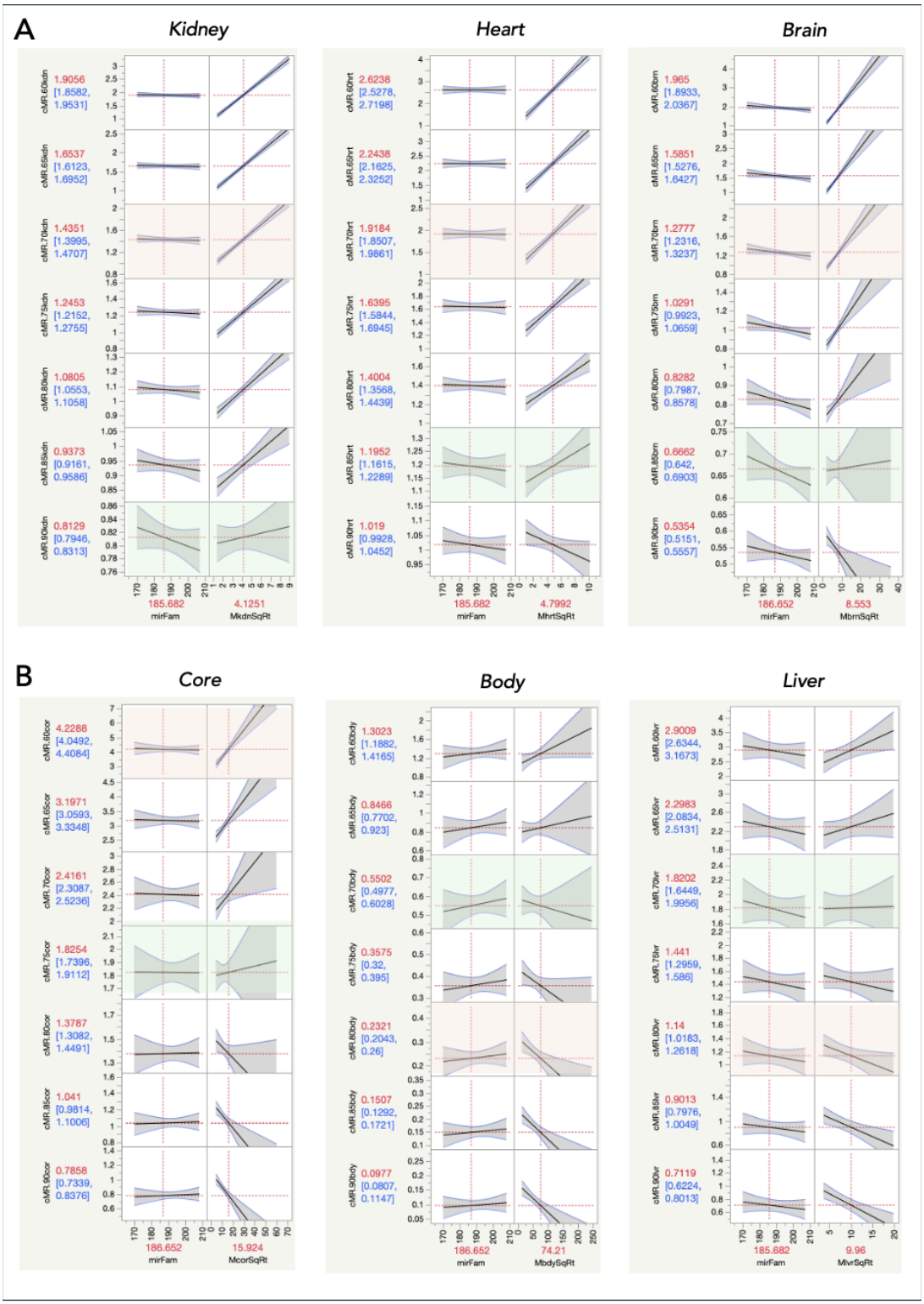

Figure 4. *cMR* slopes with respect to *mirFam* and $\sqrt{M}$, as a function of the allometric exponent (22 primates). Estimated *cMR* slopes are shaded pink, log-based *sMR* slopes are shaded green. Grey bands represent CI. Note that log-based *sMR*s correspond to crossover points for the inversions of *cMR* slope with respect to $\sqrt{M}$. A. Kidney, heart and brain *cMR*s exhibit similar patterns of slope inversion with respect to $\sqrt{M}$. B. Liver and body *cMR*s exhibit similar slope inversions with respect to $\sqrt{M}$. Only Core *cMR* slopes invert at $M^{0.75}$. Values in red represent means ± CI (blue).

(*i.e. cMR.60 - cMR.90*), revealing opposite trends for liver, on the one hand (decreasing *P* value/increasing correlation), and kidney, heart and brain, on the other (increasing *P* value/decreasing correlation) (Figure 3). Assuming an operating range of $M^{0.70}$ - $M^{0.80}$, we assigned each organ a *cMR* based on the lowest *P* value in this range, hence:

*cMR.**70**kdn*, *cMR.**70**hrt*, *cMR.**70**brn* and *cMR.**80**lvr*.

For each organ, the log-based *sMR* corresponded to the crossover point for the inversion of the *cMR* slopes with respect to organ size *i.e.* the zone of greatest mass-independent variation (Figure 4). Again, there was an obvious distinction between the allometric exponent for the slope inversions of kidney, heart and brain (~*cMR.85*) (Figure 4-A) and the exponent for the slope inversions for liver and whole body (~*MR.70*) (Figure 4-B). Only the Core *cMR* exhibited an intermediate slope inversion (~$M^{0.75}$) and log-based *sMR* ($M^{0.756}$) corresponding to Kleiber's allometric exponent for mammalian *sMR* (Figure 4-B)[30]. Given that $M^{0.75}$ is the optimal scaling for a model of stabilizing selection of mammalian *cMR* with respect to *mirFam*[4], this zone of minimal body size constraint on the Core *cMR* appears to represent an adaptive feature of the highly conserved relationship between the whole body rate of energy expenditure and body mass.

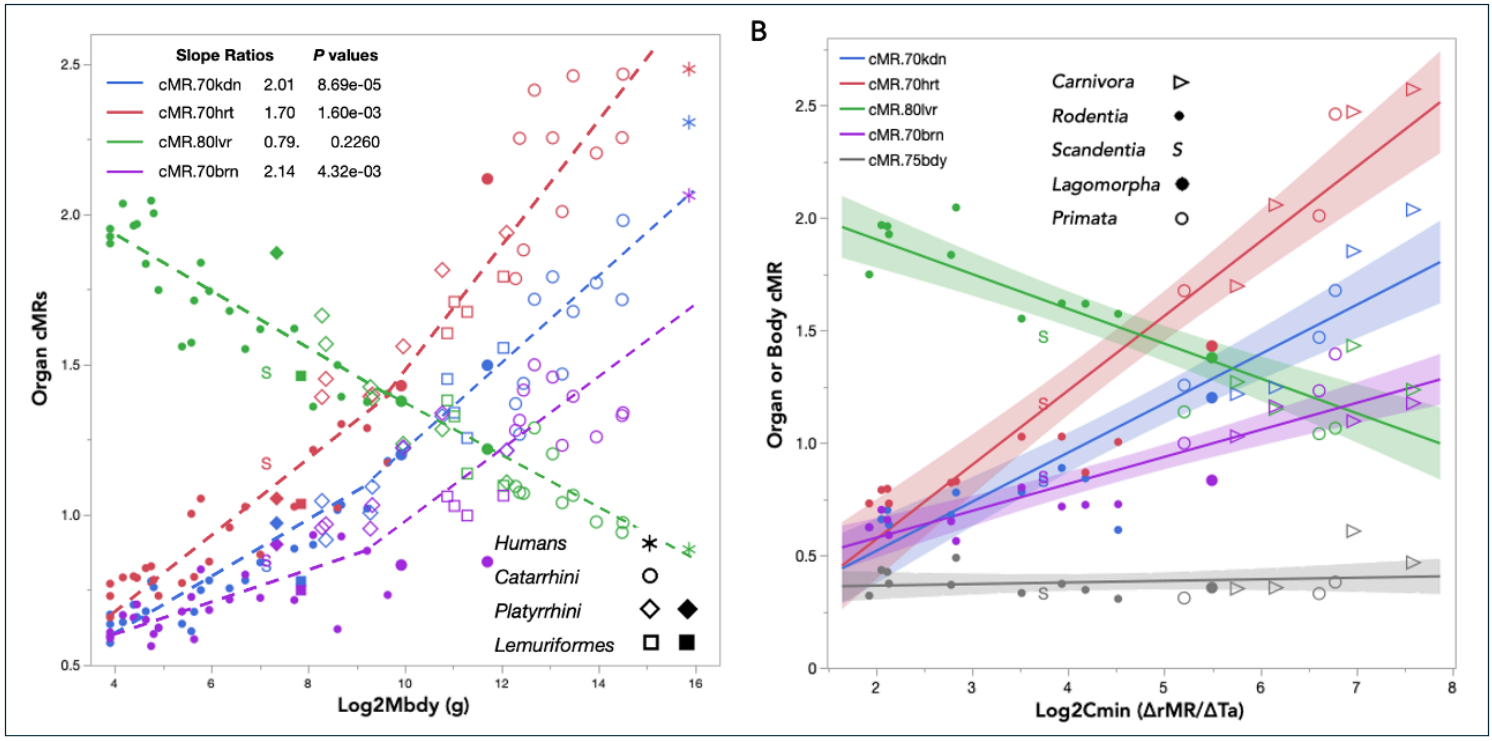

Figure 5. Core organ *cMR*s as a function of body size or thermal conductance (*Cmin*).
A. Eaurchontoglires (N = 51). Slope ratios between primates and Glires were compared by ANCOVA. Confidence intervals have been omitted for clarity.
B. Boreoeutheria (*N* = 20). T_a = ambient temperature. Shaded bands: confidence intervals (CI).

Plotting organ *cMR*s as a function of body size again revealed the inverse relationship between *cMR.80lvr* and the *cMR.70*s of the other three organs: while the latter increased directly with size, *cMR.80lvr* was strictly anticorrelated with body mass (Figure 5-A). A further distinction was that the slope of *cMR.80lvr* was unchanged between smaller-bodied Glires and larger-bodied primates, while the slopes for kidney, heart and brain *cMR.70* increased significantly from one clade to the next (Figure 5-A).

The same ranking of slopes (heart > kidney > brain) and anticorrelation with liver *cMR.80* was obtained when organ *cMR*s were regressed on the thermal conductance (C_{min}) of 20 Boreoeutheria (Figure 5-B). C_{min}, which determines the whole-body rate of heat dissipation, is an extensive property that depends primarily on total body surface area and, secondarily, on the properties of the insulating layer[25, 31]. When Boreoeutheria were ranked by the whole-body rate of heat generation (*cMR.75*), *mirFam* covaried with body size, core thermogenesis (*cMR.53cor*) and thermal conductance ($\log C_{min}$), independent of phylogenetic clade (Supplementary Figure S4-A). Ranking Boreoeutheria by C_{min} revealed tradeoffs between liver *cMR.80*, on the one hand, and both brain and heart *cMR.70*, on the other (Supplementary Figure S4-B). These relationships reinforce the notion that *mirFam*-based *cMR*s evolved in relation to body size and thermal homeostasis.

Thermodynamic and phylogenetic relevance of Core organ cMRs

We tested two predictions, the first derived from the allometric model that is the basis of the *rMR*s in our dataset[32], and the second from the thermoregulatory core model of Porter and Kearney (2009)[25]:

i) The joint *sMR* of the thermogenic organs should scale as $M^{0.75}$, since the individual organ *rMR*s were inferred from an additive model assuming that whole body $sMR = 70 \times M^{0.75}$ [32]. We disregard the "residual" metabolic rate, which averaged only 4.5% that of the liver in mammals < 75 kg[32];

ii) The joint *cMR* of the four most highly thermogenic organs, although delocalized, should scale approximately as the geometrically centered, thermogenic core of the biophysical model *i.e.* ~ $M^{0.50}$. Applying partial least squares regression[33], we generated additive models in order to predict the optimal scaling of a joint Core *cMR* composed of either *mirFam*-based *cMR*s:

$$cMR.Xcor = (rMRkdn + rMRhrt + rMRlvr + rMRbrn) / (Mkdn + Mhrt + Mlvr + Mbrn)^X$$
$$= (a \cdot cMR.\mathbf{70kdn}) + (b \cdot cMR.\mathbf{70hrt}) + (c \cdot cMR.\mathbf{80lvr}) + (d \cdot cMR.\mathbf{70brn})$$

or log-based *sMR*s:

$$sMR.Xcor = (rMRkdn + rMRhrt + rMRlvr + rMRbrn) / (Mkdn + Mhrt + Mlvr + Mbrn)^X$$
$$= (a' \cdot sMR.\mathbf{90kdn}) + (b' \cdot sMR.\mathbf{87hrt}) + (c' \cdot sMR.\mathbf{67lvr}) + (d' \cdot sMR.\mathbf{83brn})$$

Among primates, the composite *cMR* model exhibited two peaks, one on either side of the inversion of Core *cMR* slopes with respect to √M: a broad peak centered at $M^{0.53}$, similar to that predicted by the biophysical model of core thermogenesis[25], and a second peak between $M^{0.80}$ - $M^{0.85}$ (Figure 6-A). The log-based joint *sMR* exhibited a single sharp peak at $M^{0.75}$, corresponding exactly to the whole-body *sMR*s of both the Core model[25] and the model from which the organ *rMR*s were derived[32]. Importantly, the *cMR* and *sMR* models exhibited critical differences in *VIP* statistics (*Variable Importance of Projection*), a measure of the number of variables constraining each model (Figure 6-A, bottom)[34], analogous to principal components. In the range *cMR.55cor* - *cMR.70cor*, only the *cMR* models depended on all four organ *cMR*s (Figure 6-A). Significantly, when scaled to $M^{0.75}$, both the *cMR* and *sMR* models of the Core were unconstrained by kidney, heart or brain *cMR*, depending only on the *cMR* of the liver (Figure 6-A, bottom).

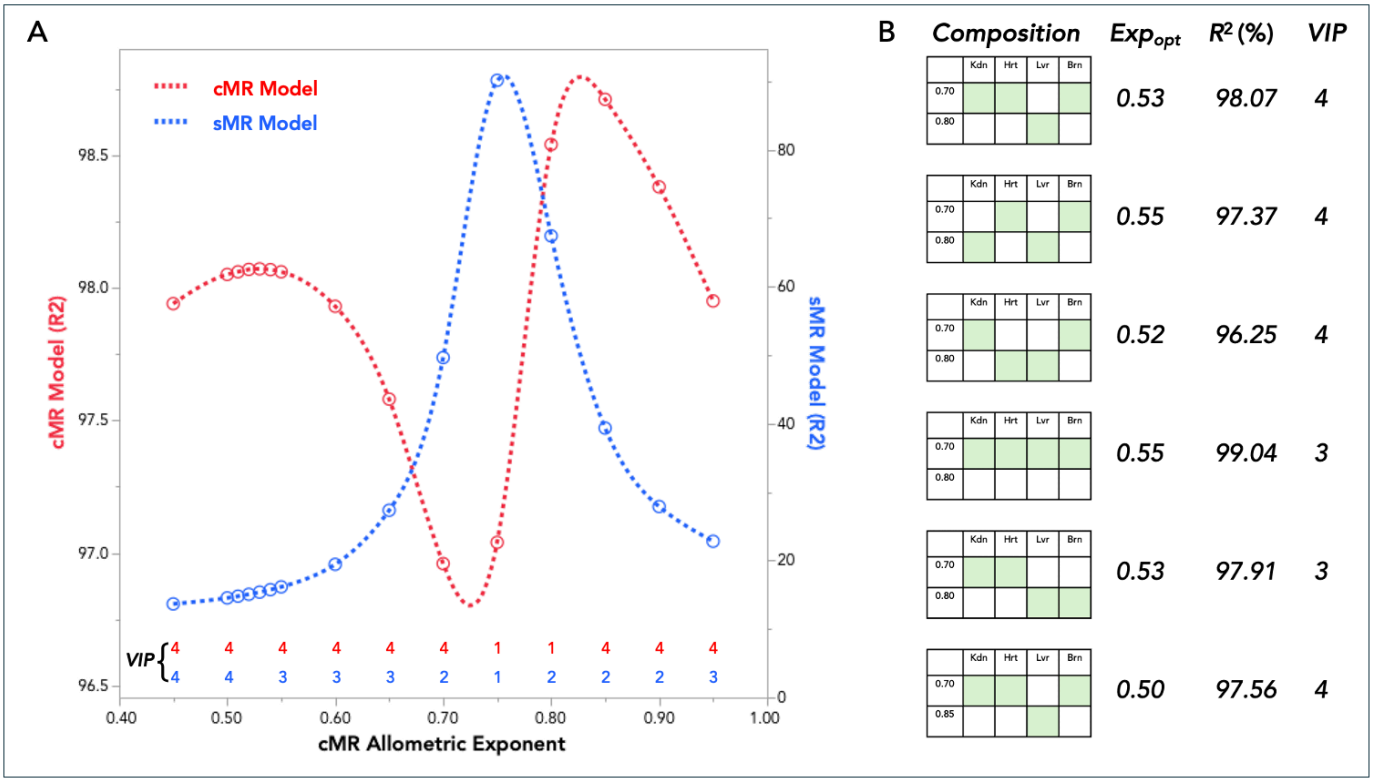

Figure 6. Variation of the primate *cMRcor* predicted by linear combinations of the *mirFam*-based *cMR*s or log-based *sMR*s of the four thermogenic organs (N = 22). Note the difference between the ranges.
A. Comparison between the *mirFam*-based *cMR* model and log-based *sMR* model. Below the plot, the table of values for *VIP* (*variable importance of projection*) indicates the number of organs upon which each model depends[34]. Curves were fit empirically using the cubic spline method (see Methods).
B. Comparison of the joint *cMR* of combinations of *cMR.70* and *cMR.80* among the four thermogenic organs. "*c*" is the organ *cMR* allometric exponent. Exp_{opt} is the optimal allometric exponent of the additive model.

We applied an additional test of the relevance of the estimated organ *cMR*s by comparing the joint *cMR*s obtained by permuting combinations of estimated organ *cMR*s, yielding four models with *VIP* = 4 (Figure 6-B).

Of these, two combinations were able to resolve Platyrrhini from Lemuriformes in an unsupervised classification of major primate clades[35]: either *cMR.80* or *cMR.85* for liver, together with *cMR.70* for heart, kidney and brain. When the liver *cMR* was varied between *cMR.75* - *cMR.85*, the original set of *mirFam*-based *cMR*s yielded the lowest value for the Bayes information criterion (BIC) (Supplementary Figure S5), hence the following optimal model of the Core *cMR*:

$$\textbf{cMR.53cor} = 0.53 \cdot \textbf{cMR.70kdn} + 0.69 \cdot \textbf{cMR.70hrt} + 0.37 \cdot \textbf{cMR.80lvr} + 0.09 \cdot \textbf{cMR.70brn}$$

In the context of the evolution of thermal homeostasis, the coefficient of each organ *cMR* in this model indicates the degree to which it has been constrained by natural selection, *i.e.* the smaller the coefficient, the greater the permitted variation of the organ *cMR* since clade divergence.

The original biophysical model for thermoregulation assumed that metabolic heat emanates from the geometric center of an ellipsoid endotherm. Depending on the wind condition or the presence of fur, the authors derived a single allometric exponent between 0.46 - 0.58 to scale the rate of core thermogenesis across the entire range of body size[25].

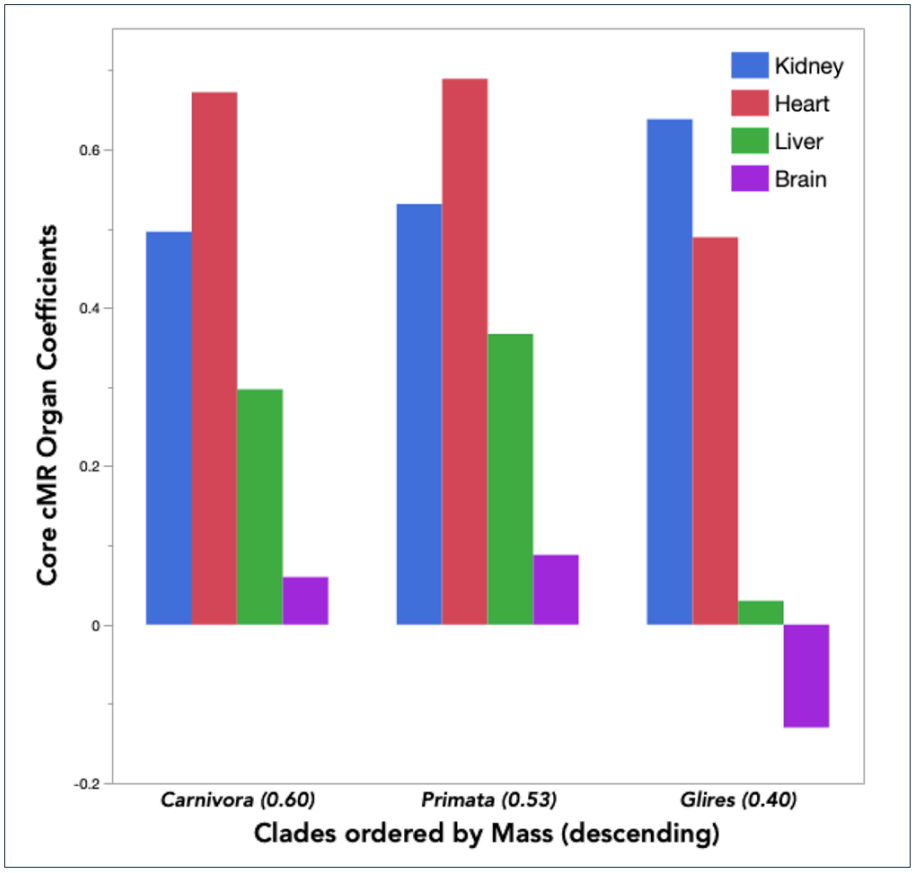

Figure 7. Organ coefficients of additive Core models in three major clades of Boreoeutheria. Values in parentheses next to each clade indicate the optimal allometric exponent of each Core *cMR* model.

236 Since our Core model is delocalized among four thermogenic organs and makes no geometric assumptions,
237 we expected lower allometric exponents ("c") and higher rates of thermogenesis (rMR/M^c) in smaller
238 mammals with higher ratios of surface area/volume. Consistent with this expectation, the optimal allometric
239 scaling of Core models developed in Carnivora, Primata and Glires were $M^{0.60}$, $M^{0.53}$ and $M^{0.40}$, respectively
240 (Figure 7). Supporting this interpretation, we find that Glires occupy the upper end of the range of *Mcor*/*Mbdy*
241 ratios, suggesting an adaptation to maintain body temperature, while primates and carnivores occupy the
242 lower end, consistent with a constraint on the rate of heat dissipation (Supplementary Figure S6-A).
243
244 The coefficients in the Glires Core model present a striking contrast with those of carnivores and primates: a
245 reversal in sign of the coefficient for brain *cMR* in Glires, and a reversal of the relative magnitudes of the
246 coefficients for liver and brain (Figure 7). The observation that the Glires model penalizes the *cMR* of the brain
247 suggests adaptation to a disproportionate reduction of body size relative to brain size, leaving the median and
248 average ratios of *Mbrn*/*Mbdy* higher in Glires than in primates or carnivora ($P < 0.001$, analysis of means)
249 (Supplementary Table S3). These arithmetic ratios represent the relative energy cost *in the individual animal*,
250 and their clade rank order is contrary to the rank order of the slope of log *Mbrn*/log *Mbdy*, which does not
251 reflect the relative energy cost of the brain *in the individual animal* (Supplementary Table S3).
252
253 ***Phylogenetic tradeoffs among cMRs validate the Core model of thermoregulation***
254 The preceding evidence suggests that Boreoeutheria have maintained thermal homeostasis while diversifying
255 in body mass by fine-tuning the relative sizes and metabolic rates of the four Core organs, particularly those
256 of the liver. We applied Bayesian inference in order to investigate the historical timing of the corresponding
257 tradeoffs. In agreement with the organ *cMR* models, we found opposite directions of evolution between the
258 organ *cMR.70*s that varied with body size, on the one hand, and *cMR.80lvr*, on the other, both upon the
259 divergence between primates and Glires, and again within each clade (Figure 8).
260
261 Among primates, an accelerated increase in liver *cMR* accompanied the decrease in size of two of the
262 smallest Platyrrhini, one of which (*Callithrix pygmaea*) may be heterothermic[36]. A clade of five small (< 1.0 kg)
263 Platyrrhini exhibited an accelerated *decrease* in brain *cMR.70* paired with elevated levels of *cMR.80lvr*,
264 consistent with adaptation to a low energy regime and increased reliance on gluconeogenesis. Among Glires
265 as well, those species that underwent the most severe reduction in size exhibited the greatest increases in
266 liver *cMR.80*; conversely, the largest-bodied clades within Glires (Lagomorpha) and Haplorhini (Catarrhini)
267 exhibited the lowest liver *cMR*s (Figure 8).

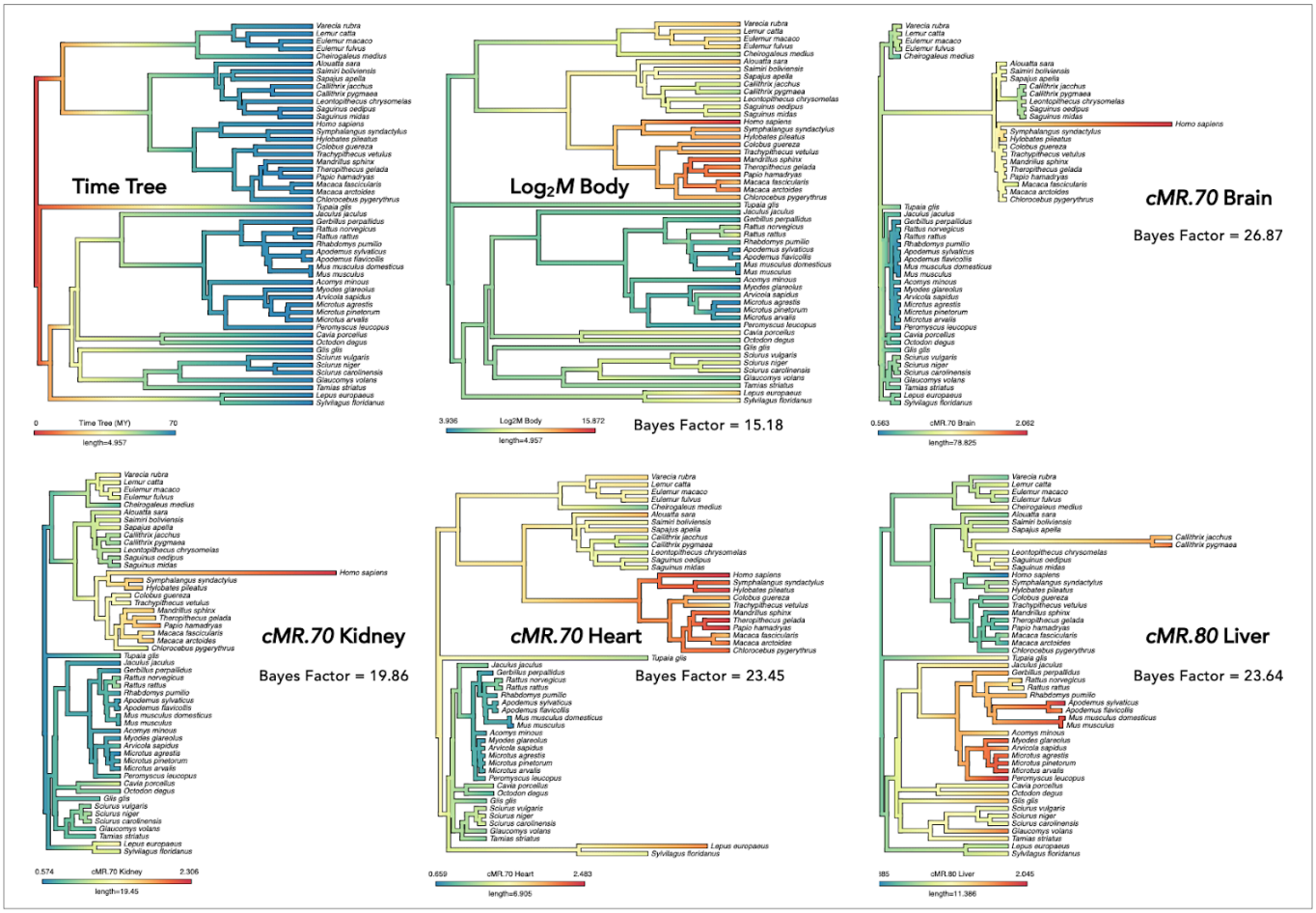

Figure 8. Variable rate phenograms of *Log Mbdy*, *cMR.80lvr*, and *cMR.70* of kidney, heart and brain. The color values applied to the reference ultrametric tree simply depict the remaining fraction of total branch length[26]. Bayes factors were computed from the difference in log likelihood (*Lh*) of the 1% most likely trees and the trees with the smallest non-zero sum of changes to branch length, *i.e.* those trees most similar to the reference time tree[4].

Brain *cMR.70* increased in intensity and its rate of evolution accelerated with the divergence of Haplorhini, and then again with humans, in contrast to its relative stasis or decrease among Glires, Lemuriformes and smaller Platyrrhini (Figure 8). The relative levels of heart *cMR.70* generally tracked body size, with accelerated rates of heart evolution in the clades of the largest Glires (Lagomorpha) and primates (Catarrhini). In addition to the accelerated evolution of brain *cMR*, the divergence of humans was marked by the accelerated rate of evolution of the *cMR.70* of the kidney (Figure 8), an observation that is noteworthy for two reasons:

a) The 30% higher level of kidney *cMR* found in humans relative to other hominoid apes is not apparent when kidney *MR* is scaled according to the slope (0.90) of log *rMRkdn*/log *Mkdn* – the value for the kidney *sMR* in humans is 10% *lower* than the average value among apes.

b) The adaptive increase in *cMR.70kdn* is of particular interest since the ability to thermoregulate is highly dependent on water balance, as illustrated in a study of baboons that, like humans, are diurnally active

and whose fossils appear in the same arid horizons as the fossils of *Australopithecus*[37] and *Homo*[12]. When free-ranging baboons were deprived of water and exposed to elevated ambient temperatures, they developed a progressive hyperthermia – with core temperature increasing on each day water was withheld – that was rapidly reversed upon rehydration[38].

DISCUSSION

The inference of cellular metabolic rates and relative brain size

The body mass and *MR* of mammals are extensive properties that vary over six orders of magnitude. The average rate of thermogenesis is an intensive property with a normal distribution that ranges only twofold, like the physical and ecological factors to which it has adapted, notably the Q_{10} coefficient for body temperature.

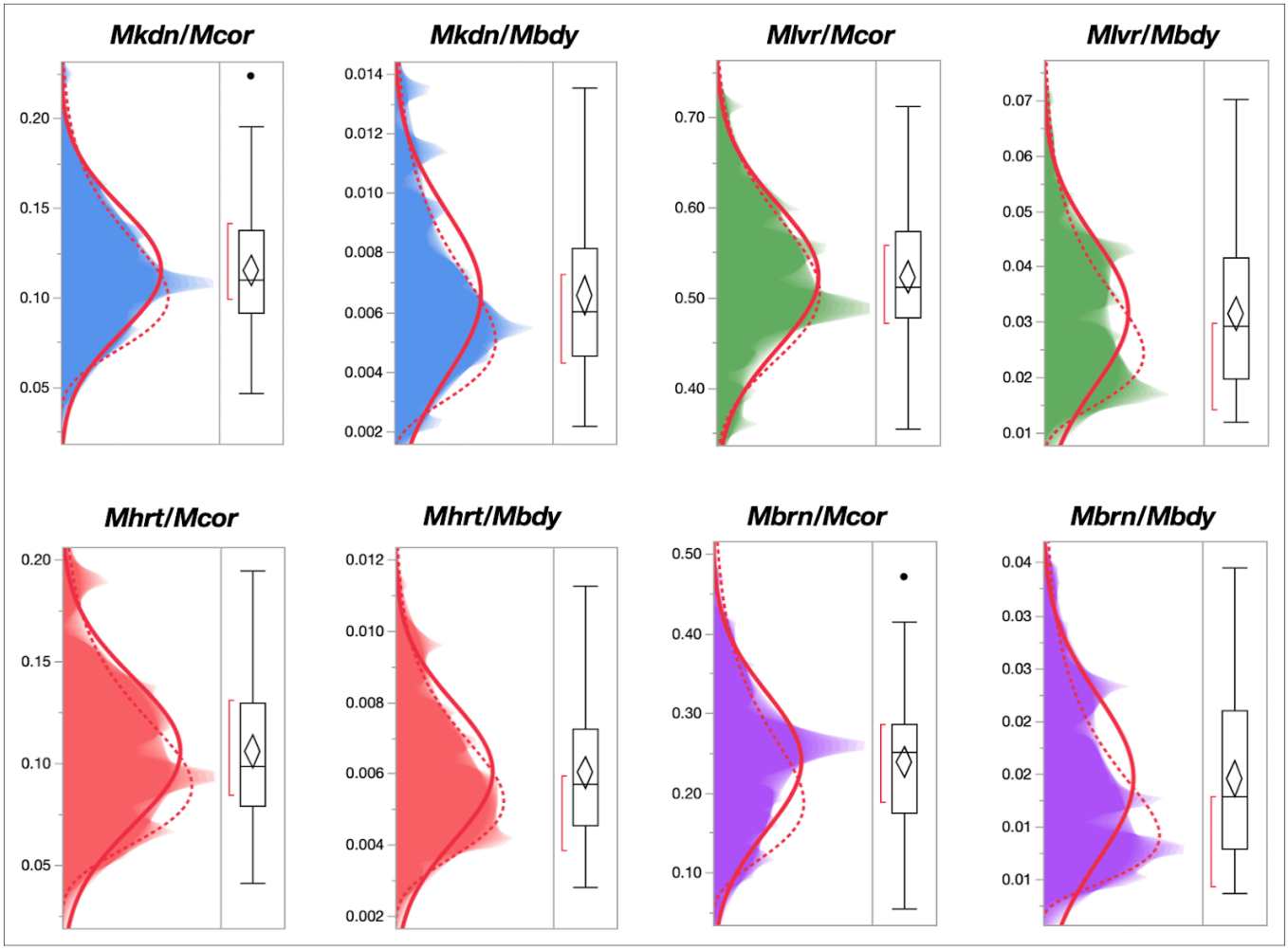

Figure 9. Distributions of the organ/Core and organ/body mass ratios in three orders of Boreoeutheria. The solid and dotted curves represent the fitted normal and lognormal distributions, respectively. The outlier box plots represent the interquartile range, confidence interval (diamond), and highest density range (50% of the observations: red bracket). All organ/Core mass ratios conformed to a Normal distribution, while in each case, the distribution of organ/body mass ratios deviated significantly from normality ($P < 0.005$, Shapiro-Wilk test). After removal of outliers from the organ/body ratios of each clade, the data for each organ represent 73 - 79 of 80 Carnivora, Glires, and Primata.

In order for the variation of trait to reveal a tradeoff among thermogenic organs, two conditions must be met: it must exhibit a normal distribution and it must represent the relative energy cost *in the individual animal*. Organ/Core mass ratios are proportional to the relative energy cost in the individual animal and exhibit a normal distribution (Figure 9). Organ/body mass ratios vary logarithmically and provide a less sensitive measure of the relative energy cost (Figure 9). The conventional index of brain size, log *Mbrn*/log *Mbdy*, does vary normally, but it does not reflect the relative energy cost *in the individual animal*. Therefore, the previous inability to detect thermoregulatory tradeoffs is the result of a category error.

Like organ/Core mass ratios, the ratios of Core mass/body mass vary normally (Supplementary Figure S6-A). These ratios are therefore amenable, without log transformation, to parametric statistical analysis and phylogenetic comparative methods. Moreover, even for allometric scaling purposes, comparison of the distributions of log *Mbrn*/log *Mcor* and log *Mbrn*/log *Mbdy* illustrates the greater resolution obtained by standardizing with respect to Core mass, rather than with respect to body mass (Supplementary Figure S6-B).

The clade rank order of mean or median *Mbrn*/*Mbdy* contradicts the clade rank order of log-based allometric slopes, leading to different interpretations of evolutionary change, with implications for covariance models of evolution[39-41]. *Mbrn*/*Mbdy* ratios and thermodynamic models of Core *cMR* indicate that the divergence of Glires from primates, as well as of Platyrrhini from Catarrhini, represent disproportionate decreases in body size with respect to brain size, consistent with the interpretation of Smaers et al (2021)[42].

Phylogenetic comparative analyses of *rMR* or *Mbrn versus Mbdy* have relied on log transformation in order to linearize these relationships, but large datasets have made it apparent that they remain curvilinear even when logged[28, 43]. Venditti et al (2024) found that a quadratic function best fit the relationship between log *Mbrn* and log *Mbdy* in a 1,500-species dataset: for a given change in body size, the brain size of the largest mammals changed approximately 40% less than that of the smallest mammals[28]. This sublinearity appears to reflect a geometric constraint: adding 1.0 g to a 9.0 g brain as part of a 20 g gain in the mass of a 200 g mammal is offset by a greater increase in surface area than the addition of 1.0 g to a 99 g brain accompanying a 20 g gain in the mass of a 2,000 g animal.

The ratio *rMRbrn*/*Mbrn* is an even more direct target of selection for thermal homeostasis than is *Mbrn*/*Mbdy*. *Regardless of phylogeny*, this ratio decreases strictly as an exponential function of body mass, consistent with surface area considerations (Supplementary Figure S7):

$$rMRbrn/Mbrn = 1.2 \cdot (\log_{10} Mbdy)^{-0.32} \qquad R^2 = 1.00 \qquad P = 0.00 \qquad (N = 51)$$

The strength of this relationship implies that as major clades of Boreoeutheria diversified in size, the energy consumption of the brain evolved in a manner that prioritized thermal homeostasis, regardless of the degree of sophistication of cognitive function.

Metabolic efficiency and the evolution of organ size

The present study demonstrates that the conserved allometric scaling of mammalian *cMR* or *sMR* ($Mbdy^{0.75}$) corresponds to a zone of minimal constraint by body size on the composition of the 4-organ Core, consistent with our original hypothesis. The observation that the slope of the regression of *cMR.80lvr* on body size has remained constant across clades, unlike the slopes of *cMR.70* for kidney, heart and liver, suggests a hierarchy of organ size regulation: *across major clades*, liver size and activity have been developmentally programmed to track body size, which varies geometrically; *within clades*, thermal homeostasis has been maintained by adjusting the relative proportions of the other three organs in the thermogenic Core (Figure 10).

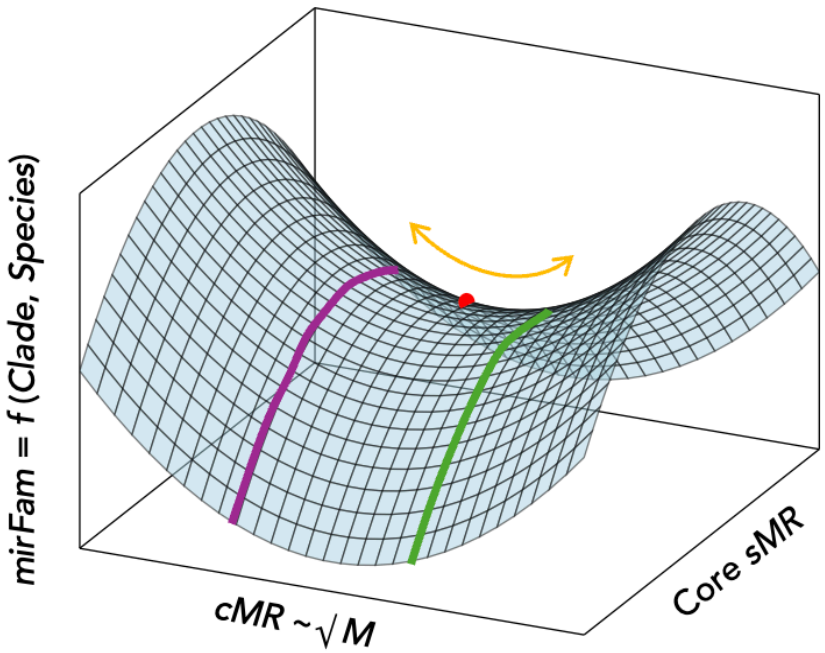

Figure 10. Conceptual summary of relationship of *mirFam* to organ *cMR*s and the Core *sMR*. Organ *cMR*s are displaced from the zone of minimal mass dependence defined by the Core *sMR*. Brain (purple) and liver (green) *cMR*s exhibit opposite patterns of correlation with body size.

Figure 10 summarizes the relationship between the number of microRNA families, organ *cMR*s and the Core *sMR*. In addition to potentially ensuring synchrony among GRNs, the clade-wide expansions of the microRNA-target apparatus that accompanied major increases in *MR*s may have served to maintain metabolic efficiency by limiting the increased expression noise associated with faster rates of protein

synthesis[44]. Protein synthesis drives 20% of ATP turnover in mammalian cells[45], and global microRNA activity has been estimated to reduce the overall rate of translation by 25%[4]. The rates of translation of low- and high-abundance mRNAs conform to the predicted outcome of global microRNA activity[46] and appear to have evolved under an energy efficiency constraint[47]. This global reduction of expression noise is best understood in the context of the 10- to 100-fold higher thermodynamic cost per gene of translation, relative to transcription[48-49], suggesting that the saddle function represents an energy efficiency landscape (Figure 10).

The developmental and phylogenetic plasticity of the liver

Since the study of Lande (1979)[24], it has been the convention to base the allometry of brain size on whole body mass. This approach has not detected significant anticorrelations among organ sizes[23], perhaps not surprisingly, considering that all organs must be developmentally programmed to track body mass[50]. The inverse relationship in the Core between brain and liver, each accounting for 20% of *bMR* in humans, is the most significant and highly conserved tradeoff, and this plasticity that appears to be an inherent property of the mammalian evolutionary toolkit, not exclusive to homeotherms. A similar inverse relationship between gluconeogenesis and the rate of body mass growth in humans implicates the liver as the pivotal partner in an ontogenetic tradeoff: brain glucose utilization peaks around age five, early in the extended period between weaning and sexual maturity, which corresponds to the period of slowest growth in body mass[51]. Based on the turnover of isotopically-labeled glucose, liver glucose production was proportional to brain mass over the entire lifespan, and therefore highest per body mass among young children[52]. Among prepubertal children (7 - 9 years of age), the rate of gluconeogenesis was still 50% higher than that found among adolescents[53].

The evolutionary plasticity of the liver appears to have co-opted the liver's inherent developmental plasticity: among mammalian organs, only the liver retains full regenerative potential[50]. If the evolution of liver mass has been determined by the demand for glucose production, then a situation of high energy reliability/low dependence on gluconeogenesis in an incipient clade may have favored evolutionary decreases in relative liver size and thermogenesis, such as those associated with the divergence of Lagomorpha from Glires, and of Catarrhini from Haplorhini. Conversely, smaller bodies and tradeoffs favoring the liver appear to signify adaptation to limited energy resources relative to population size, as exemplified by the divergence of Glires from Euarchontoglires, Strepsirrhini from primates, and Platyrrhini from Haplorhini.

Hippo-YAP, the regulator of organ size in Bilateria[54], coordinates liver growth with the suppression of gluconeogenesis[55-58]. Significantly, the global underexpression of microRNAs that is frequently observed in

tumor cells has been attributed to aberrant density-dependent regulation of the same Hippo-YAP signaling[59-60]. At low cell densities, Hippo signaling is normally suppressed, allowing YAP to localize in the nucleus and stimulate cellular proliferation, while at normal organ size and tissue density, YAP translocation and activity are normally inhibited by Hippo[54]. In contrast, constitutively active YAP suppresses microRNA levels in cells and tumors and post-transcriptionally induces oncogenic MYC protein[60]. An overall decrease in microRNA levels would be expected to cause dysregulation of gene regulatory networks (GRNs), either by disrupting the timing of transient signals, such as transcription factors[7, 61], or else by shifting the repression profile of targets regulated by multiple microRNAs[46]. By extension, the evolutionary plasticity of the liver implies repeated resetting of the dynamic ranges for the interactions among Hippo-YAP signaling, organ size, and the rate of microRNA biogenesis.

A feedback model for brain size and energy reliability

We modeled a simple feedback loop based on the inverse association between larger brain sizes and *mirFam* and lower liver sizes and *cMR*s. Assuming that the latter reflects decreased dependence on gluconeogenesis: a larger brain size leads to greater energy reliability which, in turn, facilitates the evolution of a larger brain, up to the limits imposed by anatomy and physiology, such as the diameter of the birth canal or the physiological limit on the rate of heat dissipation[62-64]. We applied a logistic feedback function to fit the distribution of *mirFam*, a proxy for energy reliability, to the primate brain size dataset of Grabowski et al (2023)[65]:

$$\frac{d\,(mirFam)}{d\,(\log V_{brn}/\log M_{bdy})} = r \cdot mirFam\,(1 - mirFam/mirFam_{max}),$$

where r is the growth rate, and the range of *mirFam* has been scaled to a range of 1.0.

As shown in Figure 11-A, log *Mbrn*/log *Mbdy* is a predictor of *mirFam,* rather than the converse, consistent with the notion that evolutionary increases in brain size tended to result in greater energy reliability. Since the distribution of *mirFam* can be fit to the mass log ratios of any thermogenic organ, we asked which relationship might be the principal target of selection. However, *mirFam* variation with respect to any trait is always secondary to phylogenetic distance, given that the ranges of *mirFam* are highly clade-specific (Supplementary Figure S7). Instead, we compared the reverse dependence on *mirFam* of organ *cMR*s. All potential kidney and heart *cMR*s (*cMR.60* - *cMR.80*) varied independently of phylogenetic distance (Pagel's *lambda* = 0.0), as did all but one liver *cMR* (*cMR.60lvr*) (Supplementary Table S4). In contrast, brain *cMR* variation with respect to *mirFam* was, in every case, secondary to phylogenetic distance (*lambda* = 1.0), *i.e.* the divergence of primate clades coincided with changes that occurred in *mirFam* range specifically with respect to brain *cMR*.

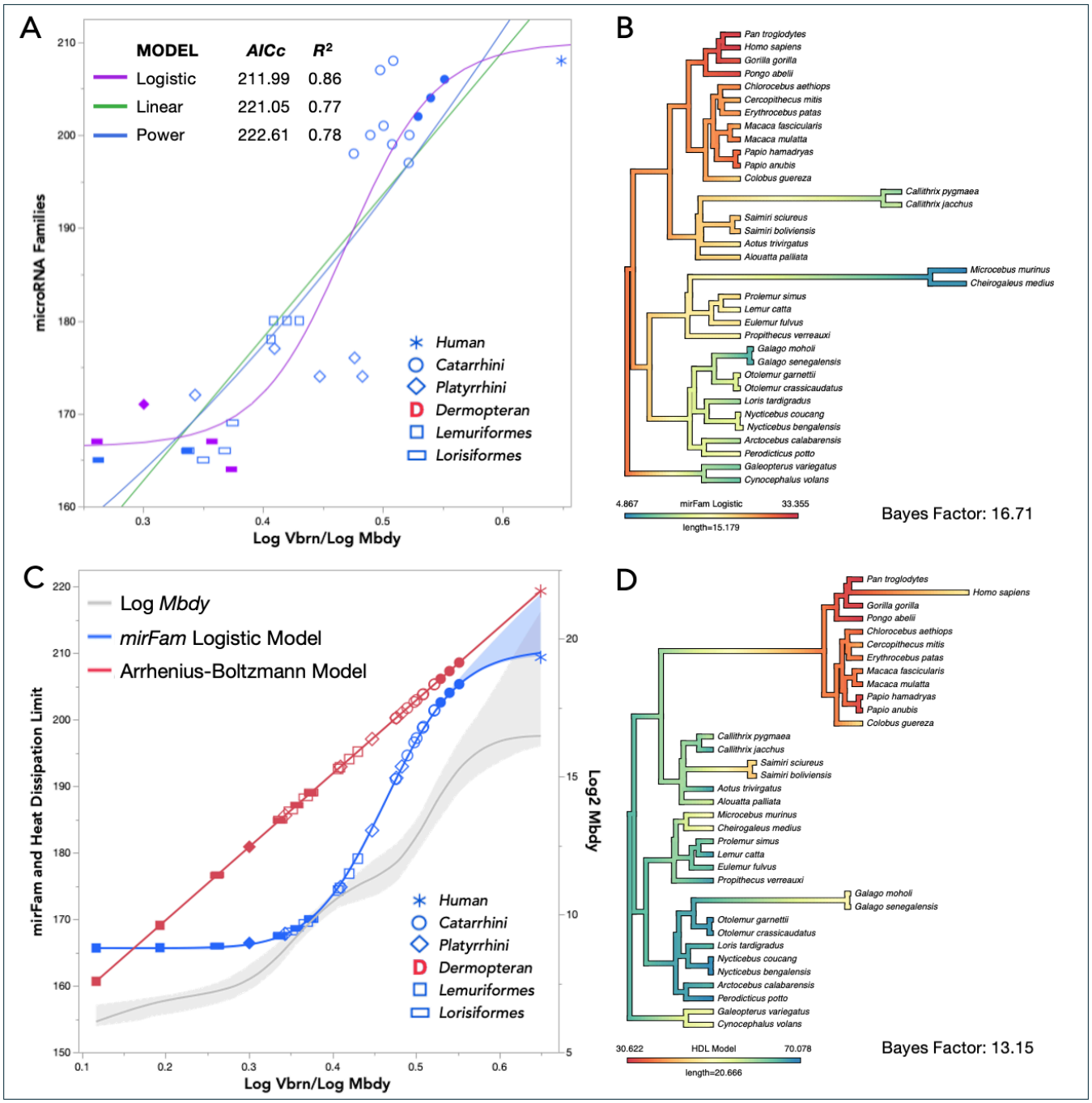

Figure 10. Logistic model of the *mirFam* relationship to relative brain size and the primate heat dissipation limit. A. Comparison of the logistic model with linear and power law models (N = 31, excluding the clade of heterothermic Cheirogaleidae: *M. murinus* and *C. medius*). Filled symbols: circles = Hominidae; rectangles and diamond: documented (blue) and suspected (purple) heterotherms. B. Variable rate phenogram based on the linearized values of the logistic model: when ranked in ascending order, the ratio of *mirFam* values to the cumulative sum decreases in a linear manner (Hubbert, 1982)[66]. C. Comparison of the logistic models with the maximal rate of thermogenesis predicted from whole-body mass and T_b (Allen et al, 2006)[67] and scaled to the same range as *mirFam*. Shading represents the CI (cubic spline method). D. Variable rate phenogram based on the difference between predicted *mirFam* and predicted HDLs. The resulting distribution was centered and the outlier clade of dwarf and mouse lemurs was assigned an intermediate value of 50.

434 A variable rate phenogram corresponding to this model was generated using ratios from the linearization of
435 the logistic function[66], such that the color scale signifies rank order (Figure 11-B). Catarrhini exhibited the
436 highest *mirFam* levels with respect to brain size, a relationship that evolved at the same rate as the underlying
437 rate of genomic evolution. In contrast, the three smallest-bodied clades, *Cheirogaleidae, Galago and Callithrix*
438 (marmosets) exhibited lower *mirFam* levels and an accelerated descent in rank (Figure 11-B). The latter
439 observation is consistent with the regression of the brain size allometry of Callitrichines to one more similar to
440 that of Strepsirrhini than that of Platyrrhini[42]. *Callithrix pygmaea* may also be heterothermic[36], and the *Callithrix*
441 clade also exhibited marked increases in the level and rate of evolution of liver *cMR.80*, suggesting adaptation
442 to a regime of reduced energy reliability that is characteristic of low calorie-density folivory or insectivory[68].
443 Thus, the *mirFam*-based feedback model implies that body size reduction, accompanied by greater liver size
444 and activity, has been a consistent adaptation to low energy reliability.
445
446 Supported by the previous observation that the energy consumption of the brain per unit mass decreases
447 exponentially as a function of body size, we postulated that the upper plateau of the logistic model, occupied
448 by primates with the largest bodies and relative brain sizes, would correspond to the physiological limit on the
449 rate of heat dissipation[4, 62-64]. Furthermore, when primate species are ranked by size, *mirFam* varies
450 reciprocally with inverse body temperature, $1/T_b$ (°*K*); thus, the seemingly random variation of T_b within each
451 clade appears to be tied to the variation in *mirFam*, except among the smallest heterotherms (Supplementary
452 Figure S8). The conserved nature of this reciprocity lends itself to the following formulation of a model of the
453 maximum heat dissipation limit (HDL). The relationship between whole body *rMR* and T_b can be described by
454 the Arrhenius-Boltzmann function, $e^{-E/kT}$, where *E* represents the mean activation energy of the respiratory
455 complexes and *k* is the Boltzmann constant[67]; when corrected for total body mass, this function represents
456 the maximal possible rate of thermogenesis and therefore heat dissipation, regardless of phylogeny or
457 thermoregulatory adaptations (Figure 11-C).
458
459 In order to detect adaptations that occurred in relation to this limit, we generated variable rate phenograms
460 that depict the direction and rate of evolution of the *difference* between the values of the HDL model and the
461 logistic model (Figure 11-C). In this case, the color scale signifies proximity to the HDL. Interestingly, two of
462 the clades that exhibit accelerated evolution toward the HDL represent the highest relative brain size among
463 Platyrrhini (*Saimiri*) and lowest relative brain size among Lorisiformes (*Galago*), suggesting thermoregulatory
464 adaptation at the extremes of variation (Figure 11-D) (Supplementary Table S2) (see also Figure 1-C). The
465 divergence of Catarrhini was associated with rapid evolution toward the HDL that was subsequently reversed

in two cases: the divergence of the human and colobus monkey, species that again represent the extremes of relative brain size in their clade (Figure 11-D). The apparent "cooling" in the human branch appears to reconcile the disproportionate increase in brain size with our species' unique adaptations for heat dissipation[9].

Our logistic model assigns the ancestral primate a high rank for energy reliability and a low rank relative to the HDL, a propitious combination for the founder of a new order of mammals. In many respects this model fulfills the recent call for an explanation of the distinct pattern of brain size evolution in primates "in terms of the release of a constraint or an adaptive shift that initiated escalating feedback between brain and behavior"[28]. Since this logistic model is agnostic regarding underlying mechanisms, it can also serve as a null hypothesis for comparison with the evolution of other candidate mechanisms of brain size evolution. More significantly, discovery of the tradeoff proposed four decades ago in order to account for the evolutionary expansion of brain size[21-22] depended on defining the criteria for a variable to be sensitive to thermoregulatory constraints.

SYNTHESIS

The adaptive value of repression by individual microRNAs operating in gene regulatory networks has been attributed to their ability to canalize phenotype expression by buffering the effects of environmental or allelic variation[69-70] and to set thresholds for cell fate determination, or maintain the identity of differentiated cells, by defining ranges of protein expression[71-72]. Major stages in the diversification of animal cell types, morphologies, and complexity of behavior have corresponded to significant expansions of microRNA and target repertoires[73-77]. For example, the emergence of placental mammals is marked by the appearance of 13 novel implantation-related microRNA families[78], and the cognitive sophistication of the genus *Octopus* has been linked to 34 novel microRNA families that are preferentially expressed in neural tissues[79]. However, these *post hoc* associations do not shed light on the preconditions of repertoire expansion, nor on how such enhanced traits may be related to a higher range of *mirFam*, as opposed to action of individual novel microRNAs[73]. The consistent pairing of adaptive shifts in *MR*/kg with expansions of the microRNA repertoire imply a prerequisite of a high level of energy reliability in an incipient clade. Given that *mirFam* losses have occurred much less frequently than gains[80], these observations suggest the operation of a ratchet mechanism that selects, among novel microRNAs, those that confer greater energy reliability. An analogy may be drawn to the fate of the duplicated genes of transcription factors (TF): owing to their established specificities, they are much more likely to be retained than the paralogues of non-TF genes[81].

METHODS

Physiological Data

The masses of the four thermogenic organs were obtained from the 111-species dataset of Wang et al (2012)[32], originally derived from the compilation of Navarette et al (2011)[23]. Only in humans have organ metabolic rates been measured directly[82]. Otherwise, they have been inferred by conventional allometric scaling based on organ mass of rat (all four organs), dog (liver, brain and kidney), cat and rabbit (liver)[83]. Relative brain sizes for the logistic models were obtained from Grabowski et al (2023)[65], Smaers et al (2021)[42] (human), and estimated for Dermoptera[84]

Values for thermal conductance (C_{min}) were obtained from the dataset of Fristoe et al (2015)[3], with substitution of congeneric species from the dataset of Wang et al (2012)[32]. Where C_{min} was available for two or more congeneric species, we chose the one with the mass nearest to the species in the Wang dataset. Body temperatures were obtained from the AnAge database[85] and other sources.

MicroRNA Families, *Binning*

Complements of *conserved* microRNA families were obtained from the most complete assembly for each species using the covariance model MirMachine[86], trained on the manually-curated database of microRNA genes, MirGeneDB2.1[5] (Supplementary Tables S1 and S2). For Scandentia, Lagamorpha and Rodentia, *mirFam* refers to the number of families common to Euarchontoglires. For Lorisiformes, Lemuriformes and Platyrrhini, *mirFam* refers to the number of families shared with Catarrhini. For the original regression of organ *cMR*s on *mirFam* and organ size (Figure 3), *mirFam* was binned according to natural divisions in its distribution: 141 - 161 (Scandentia and Glires), 165 - 181 (Glires, Lemuriformes and Platyrrhini), and 194 - 208 (Catarrhini) (Supplementary Figure S7).

Phylogenetic Trees and Variable Rate Phenograms

Using Mesquite © (2021) we derived ultrametric trees for 51 Euarchontoglires or 24 primates from the mammalian phylogeny of Alvarez-Carretero et al (2021)[26]. Variable rate trees and ancestral node values were inferred using BayesTraits (version 4)[87-88] (software available at www.evolution.rdg.ac.uk). Phenograms were generated using Phytools[89].

Bayes factors for variable rate trees were computed from the difference between the median of the top 1% likelihoods and the median likelihood of the 1% of trees with the smallest non-zero sum of changes to branch

length, *i.e.* those trees most similar to the reference time tree, as previously described[4]. In the case of those variable rate trees based on linearization of the logistic function[66], artifactual changes of slope at the extremes were avoided by the addition of dummy values to either end of the range.

Statistics

Linear, logistic, and partial least squares regressions[33-34] and normal mixture clustering[35] were carried out and visualized using JMP16®. All R^2 values were adjusted for the number of predictors. Other than linear and logistic regressions, curves were fit empirically using the cubic spline method, with the confidence intervals indicated by shading[90-91]. Phylogenetic linear regressions were carried out using the R: CAPER package[92].

Limitations

The three principal limitations of this study are:

i) the indirect origin of the mammalian organ *rMR*s: other than a single set of *in vivo* measurements in humans[82], all subsequent comparative studies have inferred organ *rMR*s from organ masses assuming log-based allometric slopes across humans, rats, rabbits, cats and dogs[32, 83].

ii) the small number and variable quality of the body temperature data in the AnAge database[85];

iii) underestimation of the number of conserved microRNA families by the MirMachine algorithm[86], relative to the reference, manually-curated database[5] (currently MirGeneDB 3.0). Among Boreoeutheria excluding bats, the correlation of computed values with MirGeneDB 3.0 is between 90 - 100%.

None of these factors is expected to affect the qualitative interpretation of our results.

REFERENCES

1. Boyles JG, Thompson AB, McKechnie AE, Malan E, Humphries MM and Careau. 2013. A global heterothermic continuum in mammals. *Global Ecol Biogeogr* **22**: 1029-1039.

2. Ruf T and Geiser F. 2015. Daily torpor and hibernation in birds and mammals. *Biol Rev* **90**: 891-926.

3. Fristoe TS, Burger JR, Balk MA, Khaliq I, Hof C and Brown JH. 2015. Metabolic heat production and thermal conductance are mass-independent adaptations to the thermal environment in birds and mammals. *Proc Natl Acad Sci USA* **112**: 15934-15939.

4. Fromm B and Sorger T. 2023. Rapid adaptation of cellular metabolic rate to the microRNA complements of mammals and its relevance to the evolution of endothermy. *iScience* **27**: 108740.

5. Fromm B, Høye E, Domanska D . . (many others) . . Friedländer MR and Peterson KJ. 2022. MirGeneDB 2.1: toward a complete sampling of all major animal phyla. *Nucl Acids Res* **50**: D204-D210.

6. Clarke AW, Høye E, Hembrom AA . . (many others) . . Fromm B. 2025. MirGeneDB 3.0: improved taxonomic sampling, uniform nomenclature of novel conserved microRNA families and updated covariance models. *Nucl Acid Res* **53**: D116–D128.

7. Cassidy JJ, Bernasek SM, Bakker R, Giri R, Peláez N, Bobrowska A, Bagheri N, Nunes Amaral LA and Carthew RW. 2019. Repressive gene regulation synchronizes development with cellular metabolism. *Cell* **178**: 980-992.

8. Pontzer H, Brown MH, Raichlen DA . . (many others) . . Ross SR. 2016. Metabolic acceleration and the evolution of human brain size and life history. *Nature* **533**: 390-393.

9. Yegian AK, Heymsfield SB, Castillo ER, Müller MJ, Redman LM and Lieberman DE. 2024. Metabolic scaling, energy allocation tradeoffs, and the evolution of humans' unique metabolism. *Proc Natl Acad Sci* **121**: e2409674121

10. Timmermann A, Yun KS, Raia P . . (many others) . . Ganopolski. 2022. Climate effects on archaic human habitats and species succession. *Nature* **604**: 495-501.

11. Dart, RA. *Australopithecus africanus*: the man–ape of South Africa. 1925. *Nature* **115**: 195-199.

12. Reed KE. 1977. Early hominid evolution and ecological change through the African Plio-Pleistocene. *J Hum Evol* **32**: 289-322.

13. Davies TJ, Daru BH, Bezeng BS . . (many others) . . Bond WJ. 2020. Savanna tree evolutionary ages inform the reconstruction of the paleoenvironment of our hominin ancestors. *Sci Rep* **10**: 12430.

14. Kamberova YG, Guhana SM, DeMarchisa A, Jianga J, Wright SS, Morgan BA, Sabetid PC, Tabina CJ, and Lieberman DE. 2018. Comparative evidence for the independent evolution of hair and sweat gland traits in primates. *J Hum Evol* **125**: 99–105.

15. Nybo L. 2012.Brain temperature and exercise performance. *Exp Physiol* **97**: 333-339.

16. Jessen C, Laburn HP, Knight MH, Kuhnen G, Goelst K, and Mitchell D. 1994. Blood and brain temperatures of free-ranging black wildebeest in their natural environment. *Am J Physiol* **267**: R1528–R1536.

17. Mitchell D, Maloney SK, Jessen C, Laburn HP, Kamerman PR, Mitchell G and Fuller A. 2002. Adaptive heterothermy and selective brain cooling in arid-zone mammals. *Comp Biochem Physiol B* **131**: 571-585.

18. Yablonskiy DA, Ackerman JJH and Raichle MR. 2000. Coupling between changes in human brain temperature and oxidative metabolism during prolonged visual stimulation. *Proc Natl Acad Sci USA* **97**: 7603-7608.

19. Leithner C and Royl G. 2014. The oxygen paradox of neurovascular coupling. *J Cereb Blood Flow Metab* **34**: 19-29.

20. Drew PJ. 2022. Neurovascular coupling: motive unknown. *Trends Neurosci* **45**: 809-819.

21. Armstrong E. 1983. Relative brain size and metabolism in mammals. *Science* **220**: 1302-1304.

22. Aiello LC and Wheeler P. 1995. The expensive-tissue hypothesis:
the brain and the digestive system in human and primate evolution. *Curr Anthro* **36**: 199-221.

23. Navarette A, van Schaik CP and Isler K. 2011. Energetics and the evolution of human brain size.
Nature **480**: 91-93.

24. Lande R. 1979. Quantitative genetic analysis of multivariate evolution applied to the brain: body size allometry. *Evolution* **33**: 402-416.

25. Porter WP and Kearney M. 2009. Size, shape, and thermal niche of endotherms.
Proc Natl Acad Sci USA **106**: 19666-19672.

26. Álvarez-Carretero S, Tamuri A, Battini M, Nascimento F, Carlisle E, Asher R, Yang Z, Donoghue P and Dos Reis M. 2022. A species-level timeline of mammal evolution integrating phylogenomic data. *Nature* **602**: 263-267.

27. Heldstab SA, Isler K, Graber SM, Schuppli C and van Schaik. 2022.
The economics of brain size evolution in vertebrates. *Curr Biol* **32**: R697-R708.

28. Venditti, C, Baker J and Barton RA. 2024. Co-evolutionary dynamics of mammalian brain and body size.
Nat Ecol Evol **8**: 1534–1542.

29. White CR, Marshall DJ, Alton LA . . (many others) . . and Ortiz-Barrientos D. 2019.
The origin and maintenance of metabolic allometry in animals. *Nature Ecol Evol* **3**: 598-603.

30. Kleiber M. 1932. Body size and metabolism. *Hilgardia* **6**: 315-353.

31. Scholander PF, Hock F, Walters V, Johnson F and Irving L. 1950.
Heat Regulation in Some Arctic and Tropical Mammals and Birds. *Biol Bull* **99**: 237-258.

32. Wang ZM, Zhang J, Ying Z and Heymsfield SB. 2012. Organ-tissue level model of resting energy expenditure
across mammals: new insights into Kleiber's Law. *ISRN Zool*: 673050.

33. de Jong S. SIMPLS: 1993. An alternative approach to partial least squares regression.
Chemometrics and Intelligent Laboratory Systems **18**: 251-263.

34. Wold S, Johansson E. and Cocchi, M. 1993. PLS: partial least squares projections to latent structures.
In *Drug Design: Theory, Methods and Applications* (pp. 523-550). Kluwer ESCOM Science Publisher.

35. Celeux G and Govaert G. 1995. Gaussian Parsimonious Clustering Models. *Pattern Recognition* **28**: 781-793.

36. Tattersall GJ. 2012. Diurnal changes in metabolic rate in pygmy marmosets: Implications for sleep, torpor, and basal metabolism in primates. In: Ruf, Bieber, Arnold, Millesi (eds), *Living in a Seasonal World*, chapter **41**: 471-480. Springer.

37. Brain CK. 1981. The Hunters or the Hunted?: An Introduction to African Cave Taphonomy.
Chicago University Press, Chicago.

38. Brain C and Mitchell D. 1999. Body temperature changes in free-ranging baboons (*Papio hamadryas ursinus*) in the Namib Desert, Namibia. *Intl J Primatol* **20**: 585-598.

39. Felsenstein J. 1985. Phylogenies and the comparative method. *Amer Naturalist* **125**: 1-15.

40. Hansen TF. 1997. Stabilizing selection and the comparative analysis of adaptation. *Evolution* **51**: 1341-1351.

41. Pagel M. 1999. Inferring the historical patterns of biological evolution. *Nature* **401**: 877-884.

42. Smaers JB, Rothman RS, Hudson DR . . (many others) . . Safi K. 2021. The evolution of mammalian brain size. *Sci Adv* **7**: eabe2101.

43. Kolkotrones T, Savage V, Deeds EJ and Fontana W. 2010. Curvature in metabolic scaling. *Nature* **464**: 753-756.

44. Ozbudak EM, Thattai M, Kurtser I, Grossman AD and van Oudenaarden. 2002. Regulation of noise in the expression of a single gene. *Nature Genetics* **31**: 69-73.

45. Buttgereit F and Brand MD. 1995. A hierarchy of ATP-consuming processes in mammalian cells. *Biochem J* **312**: 163-167.

46. Schmiedel JM, Klemm SL, Zheng Y, Sahay A, Blüthgen N, Marks DS and van Oudenaarden A. 2015. MicroRNA control of protein expression noise. *Science* **348**: 128-132.

47. Schwanhäusser B, Busse D, Li N, Dittmar G, Schuchhardt J, Wolf J, Chen W and Selbach M. 2011. Global quantification of mammalian gene expression control. *Nature* **473**: 337–342.

48. Wagner A. 2005. Energy Constraints on the evolution of gene expression. *Mol Biol Evol* **22**: 1365–1374.

49. Lynch M and Marinov GK. 2015. The bioenergetic costs of a gene. *PNAS* **112**: 15690-15695.

50. Penzo-Méndez AI and Stanger BZ. 2015. Organ-size regulation in mammals. *Cold Spring Harb Perspect Biol* **7**: a019240.

51. Kuzawa CW, Chugani HT, Grossman LI, Lipovich L, Muzik O, Hof PR, Wildman DE, Sherwood CC, Leonard WR and Lange N. 2021. Metabolic costs and evolutionary implications of human brain development. *Proc Natl Acad Sci USA* **111**: 13010-13015.

52. Bier DM, Leake RD, Haymond MW, Arnold KJ, Gruenke LD, Sperling MA and Kipnis DM. 1977. Measurement of "true" glucose production rates in infancy and childhood with 6,6-Dideuteroglucose. *Diabetes* **25**: 1016-23.

53. Sunehag AL, Treuth MS, Toffolo G, Butte NF, Cobelli C, Bier DM and Haymond MW. 2001. Glucose production, gluconeogenesis, and insulin sensitivity in children and adolescents: an evaluation of their reproducibility. *Ped Res* **50**: 115-123.

54. Camargo FD, Gokhale S, Johnnidis JB, Fu D,1 Bell GW, Jaenisch R, and Brummelkamp TR. 2007. YAP1 increases organ size and expands undifferentiated progenitor cells. *Curr Biol* **17**: 2054-2060.

55. Hu Y Shin DJ, Pan H, Lin Z, Dreyfuss JM, Camargo FD, Miao J, and Biddinger SB. 2017. YAP suppresses gluconeogenic gene expression via PGC1α. *Hepatol* **66**: 2029–2041.

56. Ibar C and Irvine KD. 2020. Integration of Hippo-Yap signaling with metabolism. *Dev Cell* **54**: 256-267.

57. Cox AG, Tsomides A, Yimlamai D . . (many others) . . Goessling W. 2018. Yap regulates glucose utilization and sustains nucleotide synthesis to enable organ growth. *EMBO J* **37**: e100294.

58. Driskill JH and Pan D. 2021. The Hippo pathway in liver homeostasis and pathophysiology. *Ann Rev Pathol Mech Dis* **16**: 299-322.

59. Zhao B, Wei X, Li W . . (many others) . . Guan KL. 2007. Inactivation of YAP oncoprotein by the Hippo pathway is involved in cell contact inhibition and tissue growth control. *Genes Dev* **21**: 2747-2761.

60. Mori M, Triboulet R, Mohseni M, Schlegelmilch K, Shrestha K, Camargo FD and Gregory RI. 2014. Hippo signaling regulates Microprocessor and links cell-density-dependent miRNA biogenesis to cancer. *Cell* **156**: 893–906.

61. Keuls RA, Oh YS, Patel I and Parchem RJ. 2023. Post-transcriptional regulation in cranial neural crest cells expands developmental potential. *Proc Natl Acad Sci USA* **120**: e2212578120.

62. Speakman JR and Król E. 2010. Maximal heat dissipation capacity and hyperthermia risk: neglected key factors in the ecology of endotherms. *J Anim Ecol* **79**: 726-746.

63. Araújo MB, Ferri-Yáñez F, Bozinovic F, Marquet PA, Valladares F and Chown SL. 2013. Heat freezes niche evolution. *Ecol Letters* **16**: 1206-1219.

64. Bennett JM, Sunday J, Calosi P . . (many others) . . and Olalla-Tárraga MA. 2021. The evolution of critical thermal limits of life on Earth. *Nature Comm* **12**: 1198.

65. Grabowski M, Kopperud BT, Tsuboi M and Hansen TF. 2023. Both diet and sociality affect primate brain-size evolution. *Syst Biol* **72**: 404-418.

66. Hubbert MK. 1982. Techniques of prediction as applied to the production of oil and gas. In Gass, Saul I. (ed.) *Oil and Gas Supply Modeling* (proceedings of a symposium held at the Department of Commerce, Washington, DC, June 18–20, 1980). National Bureau of Standards Special Publication **631**: 16-141. Washington (DC).

67. Allen AP, Gillooly JF, Savage VM and Brown JH. 2006. Kinetic effects of temperature on rates of genetic divergence and speciation. *Proc Natl Acad Sci USA* **103**: 9130-9135.

68. Schiel N and Souto A. 2017. The Common Marmoset: an overview of its natural history, ecology and behavior. *Dev Neurobiol* **77**: 244–262.

69. Hornstein H and Shomron N. 2006. Canalization of development by microRNAs. *Nature Genetics* **38**: S20-S24.

70. Li X, Cassidy JJ, Reinke CA, Fischboeck S and Carthew RW. 2009. A microRNA imparts robustness against environmental fluctuation during development. *Cell* **137**: 273-282.

751 71. Mukherji S, Ebert MS, Zheng GXY, Tsang JS, Sharp PA and van Oudenaarden A. 2011.
752 MicroRNAs can generate thresholds in target gene expression. *Nature Genetics* **43**: 854-859.
753
754 72. Ebert MS and Sharp PA. 2012. Roles for MicroRNAs in conferring robustness to biological processes.
755 *Cell* **149**: 515-524.
756
757 73. Zolboot N, Du JX, Zampa F and Lippi G. 2021.
758 MicroRNAs instruct and maintain cell type diversity in the nervous system. *Front Mol Neurosci* **14**: 646072.
759
760 74. Makeyev EV and Maniatis T. 2008. Multilevel Regulation of Gene Expression by MicroRNAs.
761 *Science* **319**: 1789-1790.
762
763 75. Erwin DH, Laflamme M, Tweedt SM, Sperling EA, Pisani D and Peterson KJ. 2011.The Cambrian conundrum:
764 early divergence and later ecological success in the early history of animals. *Science* **334**: 1091-1097.
765
766 76. Dexheimer PJ and Cochella L. 2020. MicroRNAs: from mechanism to organism. *Front Cell Dev Biol* **8**: 409.
767
768 77. Peterson KJ, Beavan A, Chabot PJ, McPeek MA, Pisani D, Fromm B and Simakov O. 2022. MicroRNAs as Indicators
769 into the Causes and Consequences of Whole-Genome Duplication Events. *Mol Biol Evol* **39**: msab344.
770
771 78. Taylor AS, Tinning H, Ovchinnikov V, Edge J, Smith W, Pullinger AL, Sutton RA, Constantinides B, Wang D,
772 Forbes K, Forde N and O'Connell MJ. 2023. A burst of genomic innovation at the origin of placental mammals
773 mediated embryo implantation. *Comm Biol* **6**:459.
774
775 79. Zolotarov G, Fromm B, Legnini I, Ayoub S, Polese G, Maselli V, Chabot PJ, Vinther J, Styfhals S,
776 Seuntjens E, Di Cosmo A, Peterson KJ and Rajewsky N. 2022.
777 MicroRNAs are deeply linked to the emergence of the complex octopus brain. *Sci Adv* **8**: eadd9938.
778
779 80. Tarver JE, Taylor RS, Puttick MN, Lloyd GT, Pett W, Fromm B, Schirrmeister BE, Pisani D, Peterson KJ and Donoghue
780 PCJ. 2018. Well-annotated microRNAomes do not evidence pervasive miRNA loss. *Genome Biol Evol* **10**: 1457-1470.
781
782 81. Baker EA and Woollard A. 2022. The road less travelled? Exploring the nuanced evolutionary consequences
783 of duplicated genes. *Essays in Biochemistry* **66**: 737-744.
784
785 82. Elia M. 1992. Organ and tissue contribution to metabolic rate. In *Energy Metabolism:*
786 *Tissue Determinants and Cellular Corollaries*. Kinney JM and Tucker HN (editors), pp: 19-60. Raven Press, New York.
787
788 83. Gallagher D, Belmonte D, Deurenberg P, Wang Z, Krasnow N, Pi-Sunyer FX and Heymsfield SB. 1998. Organ-tissue
789 mass measurement allows modeling of REE and metabolically active tissue mass. *Am J Physiol* **275**: E249–E258.
790
791 84. Martin RD. 1993. Primate origins: plugging the gaps. *Nature* 363: 223-234.
792
793 85. Magalhães JP, Abidi Z, dos Santos GA . . (many others) . . Ka Po To P. 2024. Human Ageing Genomic Resources:
794 updates on key databases in ageing research. *Nucl Acids Res* **52**: D900-D908.
795
796

86. Umu SU, Paynter VM, Trondsøn H, Buschmann T, Rounge TB, Peterson KJ and Fromm B. 2023. Accurate microRNA annotation of animal genomes using trained covariance models of curated microRNA complements in MirMachine. *Cell Genomics* **3**: 100348.

87. Pagel M, Meade A and Barker D. 2004. Bayesian estimation of ancestral character states on phylogenies. *Syst Biol* **53**: 673-684.

88. Venditti C, Meade A. and Pagel M. 2011. Multiple routes to mammalian diversity. *Nature* **479**: 393-396.

89. Revell LJ. 2012. phytools: an R package for phylogenetic comparative biology (and other things). *Methods Ecol Evol* **3**: 217-223.

90. Reinsch CH. 1967. Smoothing by Spline Functions. *Numerische Mathematik* **10**: 177–183.

91. Eubank RL. 1999. Nonparametric regression and spline smoothing (2nd ed). CRC. Boca Raton, Florida.

92. Orme D, Freckleton RP, Thomas GH and Petzoldt T. 2013. CAPER: comparative analyses of phylogenetics and evolution in R. *Methods Ecol and Evol* **3**: 141-151.

DECLARATIONS

Acknowledgment

BF is supported by the Tromsø forskningsstiftelse (TFS) [20_SG_BF 'MIRevolution'].

Author Contributions

Conceptualization: TS; Methodology: TS; Investigation: BF and TS; Writing – Original Draft: TS; Writing – Review & Editing: BF and TS; Visualization: TS; Funding Acquisition: BF.

Declaration of Interests

The authors declare no competing interests.

Statement on the use of AI

No part of this work was generated or edited using any Large Language Module.